Synthesis and characterization of mixed ligand complexes of lomefloxacin drug and glycine with transition metals. Antibacterial, antifungal and cytotoxicity studies

Gehad G. Mohamed [a,*], Hanan F. Abd El-Halim [b], Maher M.I. El-Dessouky [a], Walaa H. Mahmoud [a]

[a] Chemistry Department, Faculty of Science, Cairo University, 12613 Giza, Egypt
[b] Pharmaceutical Chemistry Department, Faculty of Pharmacy, Misr International University, Cairo, Egypt

ABSTRACT

Mixed ligand complexes derived from lomefloxacin (LFX, L^1) as primary ligand and glycine (L^2) as secondary ligand have been prepared and characterized by conventional techniques including elemental analyses, XRD, infrared, electronic spectra, molar conductivity and thermal analyses. The elemental analyses data display the formation of 1:1:1 [M:L^1:L^2] complexes. The diffused reflectance and magnetic moment measurements reveal the presence of the complexes in an octahedral geometry. The infrared spectral data show that the chelation behavior of the ligands toward transition metal ions is through carbonyl O, and carboxylate O of LFX whereas the amino acid coordinate through the carboxylate oxygen and the amino nitrogen. The electronic spectral results display the existence of π–π_* (phenyl rings), n–π_* (NH_2 and —C=N) and confirm the mentioned structure. The molar conductivity reveals an electrolytic nature of all chelates. The thermogravimetric analysis data of the complexes displays the existence of hydrated and coordinated water molecules. The effect of LFX, glycine and their complexes on the inhibition of bacteria or fungi growth were evaluated. The prepared complexes were found to exhibit enhanced activity on bacteria or fungi growth compared to LFX and glycine ligands. LFX, [Mn(LFX)(Gly)($H_2O)_2$]·Cl, [Co(LFX)(Gly)($H_2O)_2$]·Cl and [Zn(LFX)(Gly)($H_2O)_2$]·Cl were found to be very active against breast cancer cells with IC50 values 14, 11.2, 13 and 16.8, respectively, while glycine and other complexes had been shown to be inactive at lower concentration than 100 μg/ml.

© 2011 Elsevier B.V. All rights reserved.

1. Introduction

Metal ion-mediated reactions involving nucleic acid constituents and amino acid side chains have been the subject of several investigations [1–6]. These reactions provide an opportunity to identify the nature of such interactions *in vivo* as they serve as models for many metalloenzyme reactions. The fluoroquinolones constitute an important class of synthetic antimicrobial agents, which have been the objects of intensive study [7]. Numerous studies regarding the interaction between various quinolones with metallic cations have been reported in the literature [8–11]. These studies have been primarily directed towards the identification of functional groups directly linked to the metal and to establish the structure formed by these coordination complexes. Other investigations aim to show the effect of metal ions upon antibacterial activity [12,13]. Still, other research groups have reported the antibacterial properties of metal complexes with fluoroquinolones [14–17]. The coordination of the fluoroquinolones with metallic ions by way of the piperazine nitrogen atoms is much less com-

mon. The literature contains few examples, such as a complex of zinc whose structure was revealed by X-ray diffraction, where two molecules of the ligand norfloxacin coordinate via the ketonic and carboxylic oxygen atoms and two other molecules coordinate by way of the terminal nitrogen of the piperazine [18,19]. Lomefloxacin is a bactericidal fluoroquinolone agent with activity against a wide range of gram-negative and gram-positive organisms. Its chemical IUPAC name is 1-ethyl-6,8-difluoro-7-(3-methylpiperazin-1-yl)-4-oxoquinoline-3-carboxylic acid (Fig. 1). The bactericidal action of lomefloxacin results from interference with the activity of the bacterial enzymes DNA gyrase and topoisomerase IV, which are needed for the transcription and replication of bacterial DNA [1]. Modifications of LFX were made based on structure–activity relationships (SARs). It was discovered that a fluorine atom at position 6 and a piperazine ring at position 7 greatly enhance the spectrum of activity. Recently, a relatively new approach to the rational design of antitumor agents has been introduced based on some new quinolone molecules that display a novel mode of action [2,3].

In order to gather more information, we thought it was important to investigate the interaction of lomefloxacin and amino acid (glycine) with the biologically important metal ions, Fe(III), Cr(III), Mn(II), Zn(II), Cu(II), Ni(II) and Co(II). These complexes were

* Corresponding author.
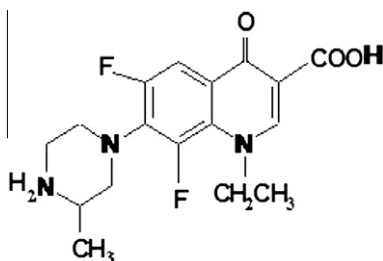E-mail address: ggenidy@hotmail.com (G.G. Mohamed).

Fig. 1. Structure of LFX drug.

prepared as models which might correspond to the complexes formed with fluroquinolone drugs *in vivo*. The complexes were characterized based on elemental analysis, conductivity data, infrared spectra, electronic spectra and magnetic susceptibility data and their bonding modes assigned. LFX acts as a neutral bidentate ligand with OO coordination sites binding under the conditions employed whereas the amino acid (glycine) acts as bidentate ligand coordinating through the carboxylate oxygen and the amino nitrogen. Octahedral geometry for metal chelates is proposed.

2. Experimental

2.1. Materials

All chemicals and reagents used in this investigation were laboratory pure (BDH, Aldrich or Sigma) including $CrCl_3 \cdot 6H_2O$, $FeCl_3 \cdot 6H_2O$, $CoCl_2 \cdot 6H_2O$, $NiCl_2 \cdot 6H_2O$, $CuCl_2 \cdot 2H_2O$, $ZnCl_2 \cdot 2H_2O$, $UO_2(NO_3)_2 \cdot 2H_2O$, $ThCl_4$, glycine, NH_4OH, DMF, C_2H_5OH and double distilled water.

2.2. Solutions

A fresh stock solution of 1×10^{-3} M LFX (0.351 g/l) was prepared in the appropriate volume of absolute ethanol. 1×10^{-3} M Stock solutions of the metal salts (Fe(III), 0.27 g/l; Co(II), 0.23 g/l; Ni(II), 0.23 g/l; Cu(II), 0.17 g/l; Zn(II), 0.172 g/l; Cr(III), 0.26 g/l; UO$_2$(II), 0.50 g/l, Mn(II), 0.16 g/l and Th(IV), 0.37 g/l) were prepared by dissolving the accurately weighed amounts of the metal salts in the appropriate volume of de-ionized water. Acid mixture (0.04 M phosphoric, acetic and boric acids) from which series of universal buffer solution of different pH values (2–12) were prepared by using 0.1 M sodium hydroxide solution for adjusting the desired pH.

Dimethylsulphoxide (DMSO) (was supplied from Sigma Chemical Co., St. Louis, Mo, and USA. It was used in cryopreservation of cells. RPMI-1640 medium (Sigma Chemical Co., St. Louis, Mo, and USA) is used. The medium was used for culturing and maintainance of the human tumor cell lines. The medium was supplied in a powder form. It was prepared as follows: 10.4 g medium was weighed, mixed with 2 g sodium bicarbonate, completed to 1 l with distilled water and shacked carefully till complete dissolution. The medium was then sterilized by filtration in a Millipore bacterial filter (0.22 μm). The prepared medium was kept in a refrigerator (4 °C) and checked at regular intervals for contamination. Before use the medium was warmed at 37 °C in a water bath and the supplemented with penicillin/streptomycin and FBS.

Sodium bicarbonate (Sigma Chemical Co., St. Louis, Mo, USA) was used for the preparation of RPMI-1640 medium. 0.05% isotonic Trypan blue solution (Sigma Chemical Co., St. Louis, Mo, USA) was prepared in normal saline and was used for viability counting. 10% Fetal Bovine Serum (FBS) (heat inactivated at 56 °C for 30 min), 100 units/ml Penicillin and 2 mg/ml Streptomycin were supplied from Sigma Chemical Co., St. Louis, Mo, USA and were used for the sup-

plementation of RPMI-1640 medium prior to use. 0.025% (w/v) Trypsin (Sigma Chemical Co., St. Louis, Mo, USA) was used for the harvesting of cells. 1% (v/v) Acetic acid (Sigma Chemical Co., St. Louis, Mo, USA) was used for dissolving the unbound SRB dye. 0.4% Sulphorhodamine-B (SRB) (Sigma Chemical Co., St. Louis, Mo, USA) dissolved in 1% acetic acid was used as a protein dye. A stock solution of trichloroacetic acid (TCA, 50%, Sigma Chemical Co., St. Louis, Mo, USA) was prepared and stored. Fifty microliters of the stock was added to 200 μl RPMI-1640 medium/well to yield a final concentration of 10% used for protein precipitation. 100% isopropanol and 70% ethanol were used. Tris base 10 mM (pH 10.5) was used for SRB dye solubilization. 121.1 g of tris base was dissolved in 1000 ml of distilled water and pH was adjusted by HCl acid (2 M).

2.3. Measurements

Microanalyses of carbon, hydrogen and nitrogen were carried out at the Microanalytical Center, Cairo University, Egypt, using CHNS-932 (LECO) Vario Elemental Analyzer. The X-ray powder diffraction analyses were carried out by using Philips Analytical X-ray BV, diffractometer type PW 1840. Radiation was provided by copper target (Cu anode 2000 W) high intensity X-ray tube operated at 4050 kV and 25 mA. Divergence and the receiving slits were 1 and 0.2, respectively. Analyses of the metals followed the dissolution of the solid complex in concentrated HNO_3, neutralizing the diluted aqueous solutions with ammonia and titrating the metal solutions with EDTA. Electronic and diffused reflectance spectra were recorded at room temperature on a Shimadzu 3101pc spectrophotometer as solutions in ethanol and solid complexes ($BaSo_4$ disk), respectively. ^1H NMR spectra, as a solution in DMSO-d_6, were recorded on a 300 MHz Varian-Oxford Mercury at room temperature using TMS as an internal standard. The molar magnetic susceptibility was measured on powdered samples using the Faraday method. The diamagnetic corrections were made by Pascal's constant and $Hg[Co(SCN)_4]$ was used as a calibrant. pH measurements were carried out using Jenway 3505 pH meter, UK FT-IR spectra were recorded on a Perkin–Elmer 1650 spectrometer ($4000–400$ cm^{-1}) in KBr pellets. The antibacterial and antifungal activities were evaluated at the Microbiological laboratory, Microanalytical center, Cairo University, Egypt. The anticancer activity was performed at the National Cancer Institute, Cancer Biology Department, Pharmacology Department, and Cairo University, Egypt. The optical density (O.D.) of each well was measured spectrophotometrically at 564 nm with an ELIZA microplate reader (Meter tech. Σ 960, USA). Molar conductivities of 10^{-3} M solutions of the solid complexes in DMF were measured on the using Jenway 4010 conductivity meter. The thermal analyses (TG, DTG and DTA) of the solid complexes were carried out from room temperature to 800 °C using a Shimadzu TG-50H thermal analyzer.

2.4. Preparation of mixed ligand complexes

The present mixed complexes were prepared by mixing equal amounts (0.01 mol) of hot saturated ethanolic solution of the first ligand (lomefloxacin) and second ligand (glycine) with the same ratio of metal chloride or nitrate salts. The mixture was refluxed for 3 h. The resulting complexes were filtered and washed several times with hot ethanol until the filtrates become clear. The solid complexes then dried in desiccator over anhydrous calcium chloride. The yield ranged from 74% to 91%.

$$M(II) \text{ or } M(III) \text{ or } M(IV) + L^1 + L^2 \rightarrow [ML^1L^2]^+$$
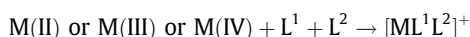
M(II) = Mn(II), Co(II), Ni(II), Cu(II), Zn(II), M(III) = Cr(III), Fe(III), M(IV) = Th(IV), L^1 = lomefloxacin, L^2 = glycine.

The dried complexes were subjected to elemental and spectroscopic analyses. The obtained complexes are soluble in ethanol, DMF and DMSO. All melting points of the complexes were measured and found to be >200 °C.

2.5. Biological activity

A filter paper disk (5 mm) was transferred into 250 ml flasks containing 20 ml of working volume of tested solution (100 g/ml). All flasks were autoclaved for 20 min at 121 °C. LB agar media surfaces were inoculated with two investigated bacteria (gram positive and gram negative) and two strains of fungi then, transferred to a saturated disk with a tested solution in the center of Petri dish (agar plates). Finally, all these Petri dishes were incubated at 25 °C for 48 h where clear or inhibition zones were detected around each disk. Control flask of the experiment was designed to perform under the same condition described previously for each microorganism but with dimethylformamide solution only and by subtracting the diameter of inhibition zone resulting with dimethylformamide from that obtained in each case, so antibacterial activity could be calculated [20]. All experiments were performed as triplicate and data plotted were the mean value.

2.6. Anticancer activity

Potential cytotoxicity of the compounds was tested using the method of Skehan et al. [21]. Cells were plated in 96-multiwell plate (104 cells/well) for 24 h before treatment with the compounds to allow attachment of cell to the wall of the plate. Different concentrations of the compounds under investigation (0, 5, 12.5, 25, 50 and 100 μg/ml) were added to the cell monolayer triplicate wells were prepared for each individual dose. The monolayer cells were incubated with the compounds for 48 h at 37 °C and in 5% CO_2 atmosphere. After 48 h, cells were fixed, washed and stained with SRB stain. Excess stain was washed with acetic acid and attached stain was recovered with tris–EDTA buffer. The optical density (O.D.) of each well was measured spectrophotometrically at 564 nm with an ELIZA microplate reader and the mean background absorbance was automatically subtracted and mean values of each drug concentration was calculated. The relation between surviving fraction and drug concentration is plotted to get the survival curve of Breath tumor cell line for each compound.

2.7. Calculation

The percentage of cell survival was calculated as follows:

Survival fraction = O.D. (treated cells)/O.D. (control cells).

The IC50 values are the concentrations of thymoquinone required to produce 50% inhibition of cell growth. The experiment was repeated 3 times for each cell line.

3. Results and discussion

3.1. UV–visible spectra of metal chelates

UV–visible spectral data of the free LFX and glycine ligands and their ternary chelates (1×10^{-3} M) solutions in aqueous universal buffer of varying pH values ranged from 2 to 12 at λ ranging from 200 to 600 nm using the same solvent as blank are studied. It is obvious that free LFX ligand gives in the neutral and alkaline media two maximum bands, the first at 325 nm and another shoulder band at 295 nm. These bands may be attributed to $n \to \pi^*$ and $\pi \to \pi^*$ transitions inside the LFX molecule. But in the acidic med-

ium the $n \to \pi^*$ transition may be disappeared due to the protonation of nitrogen atom.

It is obvious from the absorption spectra obtained that all the ternary chelates have the same behavior. The band at 320 nm may be assigned to $n \to \pi^*$ transition within the C=O group or carboxylate group of free LFX and glycine ligands. This band is red shifted to 321–326 nm in some chelates, while it disappeared in all the remaining chelates revealing the involvement of the C=O group of LFX ligand and carboxylate–O of amino acids in chelate formation [22,23].

The $n \to \pi^*$ transition within the LFX molecule is overlapped with those of glycine molecule at $\lambda = 320$–350 nm so renders it difficult to attribute the blue or red shift of these bands as a result of the involvement of the N atom of LFX or amino group of glycine during chelate formation (N $\to$ M) [22,23].

3.2. Microanalysis

The elemental analyses data of the complexes (Table 1) show the formation of the complexes in the ratio 1:1:1 for $[ML^1L^2]$. It is found that the theoretical values are in agreement with the found values.

Analytical and conductivity data of the complexes are presented in Table 1. The analytical data correspond to a metal–lomefloxacin–amino acid ratio of 1:1:1 and one mole of water per mole of metal for Fe(III) and Ni(II) complexes, two moles of water per mole of metal for Cu(II) complex and three moles of water for UO_2(II) complex.

3.3. Molar conductance measurements

From conductivity measurements, performed in dimethylformamide, it is concluded from the results given in Table 1 that the Fe(III) and Cr(III) chelates have molar conductivity values of 178 and 152 Ω^{-1} mol^{-1} cm^2, respectively, indicating that they are 1:2 electrolytes. The molar conductivity values of Mn(II), Co(II), Ni(II), Cu(II), Zn(II) and UO_2(II) chelates under investigation (Table 1) are found to be 108, 101, 126, 117, 124 and 139 Ω^{-1} mol^{-1} cm^2, respectively. It is obvious from these data that these chelates are ionic in nature and they are of the type 1:1 electrolytes. Th(IV) complex has a molar conductance value of 289 Ω^{-1} mol^{-1} cm^2, indicating its ionic nature and it is 1:3 electrolyte type.

3.4. IR spectral studies

The infrared spectra of various mixed ligand complexes synthesized are compiled in (Table 2 and Supplementary Fig. 2). The infrared spectra of these complexes in comparison with free LFX drug and the respective free glycine amino acid show characteristic band positions, shifts and intensities, which can be correlated to bidentate LFX drug and bidentate amino acid chelation. The IR spectra of the free LFX and glycine ligands and their metal complexes were carried out in the range of 4000–400 cm^{-1} and the most effective bands are listed in Table 2. The strong band observed at 1725 cm^{-1} in the free LFX ligand is assigned to the carbonyl stretching vibration [24–26]. This band is found in the spectra of the complexes at 1721–1739 cm^{-1} (Table 2) or disappeared in some complexes indicating the participation of carbonyl oxygen atom in coordination (M—O) [25]. The ν(OH), ν_{asym}(COO) and ν_{sym}(COO) stretching vibrations are observed at 3367, 1590 and 1396 cm^{-1}, respectively, for LFX free ligand [27,28,25]. Coordination with metal ions via the carboxylate O atom indicated by shift in position of ν_{asym}(COO) and ν_{sym}(COO) stretching vibration bands to 1530–1590 and 1396–1475 cm^{-1}, respectively, for LFX–Gly–metal complexes (Table 2). The ν(OH) band is still broad in all complexes, which renders it difficult to attribute to the involvement of OH group in coordination. In the 3400 cm^{-1} region,

Table 1
Analytical and physical data of LFX and its complexes with glycine.

| Compound (molecular formula) | Color (%yield) | M.p. (°C) | % Found (Calcd) | | | | μ_{eff} (BM) | Λ_m Ω^{-1} mol^{-1} cm^2 |
			C	H	N	M		
[Cr(LFX)(Gly)(H$_2$O)$_2$]·Cl$_2$ (C$_{19}$H$_{27}$N$_4$O$_7$F$_2$Cl$_2$Cr)	Dark green (91)	230	39.37 (39.03)	4.75 (4.62)	9.62 (9.59)	– (8.88)	3.55	152
[Mn(LFX)(Gly)(H$_2$O)$_2$]·Cl (C$_{19}$H$_{27}$N$_4$O$_7$F$_2$Cl Mn)	Light brown (88)	225	41.43 (41.39)	5.08 (4.90)	10.95 (10.17)	– (9.80)	5.25	108
[Fe(LFX)(Gly)(H$_2$O)$_2$]Cl$_2$·H$_2$O (C$_{17}$H$_{29}$N$_4$O$_8$F$_2$Cl$_2$Fe)	Reddish brown (85)	200	35.07 (35.05)	4.06 (4.98)	9.82 (9.62)	– (9.62)	5.82	178
[Co(LFX)(Gly)(H$_2$O)$_2$]·Cl (C$_{19}$H$_{27}$N$_4$O$_5$F$_2$ClCo)	Violet (91)	230	41.50 (41.02)	4.92 (4.86)	10.21 (10.08)	– (10.61)	5.26	101
[Ni(LFX)(Gly)(H$_2$O)$_2$]Cl·H$_2$O (C$_{19}$H$_{29}$N$_4$O$_8$F$_2$ClNi)	Light green (79)	260	38.71 (38.58)	4.86 (4.57)	9.79 (9.48)	– (9.93)	2.97	126
[Cu(LFX)(Gly)(H$_2$O)$_2$]Cl·2H$_2$O (C$_{19}$H$_{31}$N$_4$O$_9$F$_2$ClCu)	Blue (80)	200	39.79 (39.76)	5.08 (5.06)	9.83 (9.76)	– (10.29)	2.03	117
[Zn(LFX)(Gly)(H$_2$O)$_2$]·Cl (C$_{19}$H$_{27}$N$_4$O$_7$F$_2$ClZn)	White (85)	210	40.56 (40.56)	4.92 (4.80)	10.06 (9.96)	– (11.63)	Diam.	124
[Th(LFX)(Gly)(H$_2$O)$_2$]·Cl$_3$ (C$_{19}$H$_{27}$N$_4$O$_7$F$_2$Cl$_3$Th)	Pale yellow (76)	200	28.83 (28.51)	3.58 (3.38)	11.86 (11.75)	– (30.37)	Diam.	289
[UO$_2$(LFX)(Gly)](NO$_3$) (C$_{19}$H$_{23}$N$_5$O$_{10}$F$_2$U)	Yellow (74)	210	28.50 (28.25)	2.50 (2.85)	8.86 (8.67)	– (36.93)	Diam.	139

Table 2
IR spectra (4000–400 cm^{-1}) of LFX, glycine and their ternary metal complexes.

LFX	Glycine	[Cr(LFX) (Gly) (H$_2$O)$_2$]Cl$_2$·2H$_2$O	[Mn(LFX) (Gly) (H$_2$O)$_2$]Cl·2H$_2$O	[Fe(LFX) (Gly) (H$_2$O)$_2$] Cl$_2$·2H$_2$O	[Co(LFX) (Gly) (H$_2$O)$_2$] Cl·2H$_2$O	[Ni(LFX) (Gly) (H$_2$O)$_2$] Cl·H$_2$O	[Cu(LFX) (Gly) (H$_2$O)$_2$] Cl·2H$_2$O	[Zn(LFX) (Gly) (H$_2$O)$_2$] Cl·2H$_2$O	[Th(LFX) (Gly) (H$_2$O)$_2$] Cl$_3$·2H$_2$O	[UO$_2$(LFX) (Gly)] (NO$_3$)	Assignment
3367br	–	3053br	3155br	3037br	3128br	3156br	3263br	3128br	3131br	3153br	OH stretch
–	3400br	3376br	3376br	3299br	3376br	3337br	3350br	3415br	3363br	3428br	Asym. NH$_2$ stretch
–	3084br	3053s	3048s	3037s	3045s	3012s	3059s	3042br	3131br	3153br	Asym.CH stretch
–	2896s	2900s	2900s	2819s	2927s	2960s	2941s	2868s	2897s	2897s	Sym.CH stretch
–	2103m	2097s	2103m	2140s	2453m	2118s	2467m	2044s	2453s	2453s	Combination band
1725sh	1703s	1722sh	dis	dis	dis	dis	1739sh	dis	dis	dis	C=O stretch
–	1613m	1622m	1617sh	1617m	1614m	1622m	1614s	1634m	1633s	1622m	NH$_2$ scissoring
1590s	1556m	1559s	1573sh	1530s	1574s	1574m	1566s	1574m	1566s	1530s	COO asym.
1396s	1401m	1402s	1404m	1397s	1406m	1402m	1397s	1475m	1411s	1470s	COO sym.
–	1333m	1326m	1309s	1324m	1386m	1324sh	1338s	1330s	1338s	1383s	NH$_2$ twist + CH$_2$ twist
808sh	1033sh	1049sh	1052sh	1049sh	1050sh	1050sh	1052sh	1049sh	1049sh	1049sh	C—N stretch + C—C vibration
–	698sh	676s	676s	662s	658sh	659s	662s	658sh	662sh	660sh	NH$_2$ bend
–	–	574s	520s	544s	544s	574s	559s	544s	559s	558m	M—O
–	–	471s	499m	471s	456s	485s	485s	470s	441s	470s	M—O in coordinated water
–	–	411s	441s	441s	441s	456s	412s	426s	412s	427s	M—N

sh = sharp, m = medium, br = broad, s = small, w = weak.

one observes a broad absorption band due to the OH stretching of the water molecule, since, according to the elemental analysis and thermogravimetric studies, most of the complexes obtained contain water of crystallization.

As regards, chelation through amino acids, the IR spectra exhibit significant features in the νNH$_2$ and νCOO$^-$ regions. It is worthwhile to mention here that free amino acids exist as zwitterions and the IR spectra of these cannot be compared entirely with those of metal complexes as amino acids in metal complexes do not exist as zwitterions. Free amino acids with NH$_3$ functions in particular show νNH$_3$ in the range of 3130–3030 cm^{-1}. In the complexes, NH$_3$ gets deprotonated and binds to metal through the neutral NH$_2$ group. The transformation of NH$_3$ to NH$_2$ must result in an up-

ward shift in νNH$_2$ of free amino acids. At the isoelectric point, they must show νNH$_2$ in the region 3500–3300 cm^{-1} [29]. In the present complexes, the IR spectra show characteristic bands in the region 3428–3299 cm^{-1}, which are lower compared to those of free νNH$_2$. Hence, it can be concluded that the nitrogen of the amino group is involved in coordination. The IR spectra show strong evidence in support of the involvement of carboxylate group in coordination. In comparison with free amino acids, the νCOO$^-$ (asym) and νCOO$^-$ (sym) records different shifts, which confirm the monodenticity [30,31] of the carboxylate group. The values of band shift $\Delta\nu$ (ν_{asym}(COO)–ν_{sym}(COO)) are all about 143–205 cm^{-1}, indicating that the carboxylate group in glycine is chelated in a uni-negatively manner to the metal ions.

Table 3
^{1}H NMR spectral data of the lomefloxacin and its ternary chelates.

Compound	Chemical shift, (δ) ppm	Assignment
LFX	13.5	(s, H, COOH)
	8.93	(s, H, CH of carbon 2)
	7.89	(d, H, aromatic CH of carbon 5)
	3.57	(d, 4H, CH$_2$ of carbon 5′, 6′)
	3.55	(d, 2H, CH$_2$ of carbon 2′)
	3.39	(d, H, CH of carbon 3′)
	1.46	(d, 3H, CH$_3$ of carbon 1b)
	1.44	(d, 3H, CH$_3$ of carbon 3a′)
[Zn(LFX)(Gly)(H$_2$O)$_2$]·Cl	8.87	(d, H, CH of carbon 2)
	7.85	(d, H, aromatic CH of carbon 5)
	3.41	(d, 4H, CH$_2$ of carbon 5′, 6′)
	3.37	(d, 2H, CH$_2$ of carbon 2′)
	3.02	(d, H, CH of carbon 3′)
	1.46	(d, 3H, CH$_3$ of carbon 1b)
	1.44	(d, 3H, CH$_3$ of carbon 3a′)
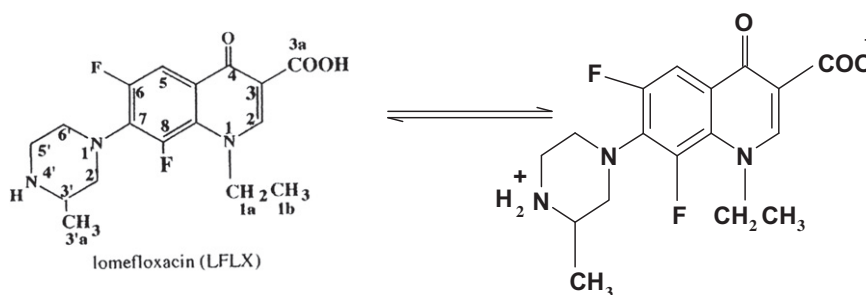
Scheme 1. Zwitter-ion formation of LFX.

Thus, it may be concluded that amino acids act as monobasic bidentates in these complexes coordinating through amino nitrogen and carboxylate oxygen [27–29]. Low intensity bands observed in far-IR region in the range 580–400 cm^{-1} are due to ν(M—O) and ν(M—N) stretching vibrations [30,31]. The metal–oxygen stretching frequencies could not be assigned unambiguously due to the presence of three types of ν(M—O) vibrations i.e., M—COO$^-$, M—H$_2$O and M—C=O. However, the data are retained in Table 2 for clarity.

Therefore, from the IR spectral studies, it is concluded that LFX behaves as a neutral bidentate ligand with OO coordination sites and coordinated to the metal ions via the carbonyl oxygen and protonated carboxylic oxygen [24–28]. Glycine behaves as a uninegative bidentate ligand with NO donor sites and coordinated to the metal ions via the amino group N and deprotonated carboxylic oxygen.

3.4.1. ^{1}H NMR spectral studies

Unfortunately, the insolubility of glycine in DMSO-d_6 make it difficult to carry out ^{1}H NMR spectrum of glycine to further clarify the way of binding of glycine ligand to the metal ions.

The proton NMR spectra of the LFX ligand and its diamagnetic Zn(II) complex were recorded in DMSO-d_6 solution using tetramethylsilane (TMS) as internal standard. The chemical shifts of the different types of protons of the LFX ligand and its diamagnetic Zn(II) complex are listed in Table 3 and represented graphically in Supplementary Fig. 3.

The comparative study of ^{1}H NMR data of free LFX ligand and its zinc complex reveals about the ligatational behavior of the ligand. Upon comparison with the free LFX ligand, the signal observed at 13.5 ppm can be assigned to the carboxylate OH. This signal disappeared in the spectrum of the Zn(II) complex. Although the LFX ligand coordinated to the metal ions without proton displacement,

the disappearance of this signal can be attributed to Zwitter-ion formation shown in Scheme 1 [19,24].

3.5. Magnetic moment measurements

The magnetic moment values are listed in Table 1. The magnetic moment values are found to be 3.55, 5.25, 5.82, 5.26, 2.97 and 2.03 BM for Cr(III), Mn(II), Fe(III), Co(II), Ni(II) and Cu(II) complexes, respectively, suggesting an octahedral geometry [23,32,33]. The Zn(II), UO$_2$(II) and Th(IV) complexes are diamagnetic. According to the empirical formulae of these complexes, an octahedral geometry was proposed.

3.6. Diffused reflectance spectral studies

A comparison of the electronic spectra of the free LFX drug and glycine ligands coordinated with those of the corresponding metal complexes, some shifts were detected. This can be considered as evidence for the complex formation. Additionally, the diffused reflectance spectra of metal complexes show different bands at different wavelengths, each one is corresponding to certain transition which suggests the geometry of the complexes. The diffused reflectance spectra of the complexes are dominated by intense intraligand charge transfer bands. The diffused reflectance spectrum of Cr(III) complex exhibits three bands at 27,411, 25,569 and 13,532 cm^{-1} which may be assigned to the $^4A_{2g}(F) \rightarrow 4T_{2g}(F)$, $^4A_{2g}(F) \rightarrow 4T_{2g}(F)$ and $^4A_{2g}(F) \rightarrow 4T_{2g}(P)$ spin allowed d–d transitions, respectively, suggesting an octahedral geometry [23,32,33]. The diffused reflectance spectrum of Mn(II) complex exhibits three bands at 25,506, 19,085 and 16,542 cm^{-1}, which may be assigned to $^4T_{1g} \rightarrow {}^6A_{1g}$, $^4T_{2g}(G) \rightarrow 6A_{1g}$ and $^4T_{1g}(D) \rightarrow 6A_{1g}$ transitions, respectively, which suggests an octahedral geometry [32,33]. From the diffused reflectance spectrum, it is observed that, the Fe(III) chelate

Table 4
Thermoanalytical results (TG, DTG and DTA) of the ternary complexes.

Complex	TG range (°C)	DTG$_{max}$ (°C)	n^*	Estim. (Calcd)%		Assignment	Metallic residue	DTA (°C)
				Mass loss	Total mass loss			
[Fe(LFX)(Gly)(H$_2$O)$_2$]Cl$_2$·H$_2$O	50–220	66	1	5.40 (5.77)		−Loss of H$_2$O		212(+), 328(−), 514(−)
	220–275	209	1	17.47 (17.14)		−Loss of 2H$_2$O and Cl$_2$	1/2Fe$_2$O$_3$	
	275–580	282, 326, 508	3	64.41 (64.28)	87.28 (86.98)	−Loss of C$_{19}$H$_{24}$F$_2$N$_4$O$_{3.5}$		
[Ni(LFX)(Gly)(H$_2$O)$_2$]Cl·H$_2$O	30–150	45	1	4.59 (3.13)		−Loss of H$_2$O		227(+), 492(−)
	150–250	224	1	24.90 (25.50)		−Loss of 2H$_2$O, HCl and C$_2$H$_4$NO$_2$	NiO	
	250–655	493	2	49.48 (50.48)	78.99 (79.11)	−Loss of C$_{17}$H$_{20}$F$_2$N$_3$O$_2$		
[Cu(LFX)(Gly)(H$_2$O)$_2$]Cl·2H$_2$O	40–115	60	1	3.69 (3.11)		−Loss of H$_2$O.		218(−), 512(−)
	115–255	199	1	22.90(21.87)		−Loss of 2H$_2$O, HCl and CH$_2$NO$_2$	CuO	
	255–695	408	2	60.35 (60.85)	86.42 (86.36)	−Loss of C$_{18}$H$_{21}$F$_2$N$_3$O$_2$		
[UO$_2$(LFX)(Gly)]·(NO$_3$)	50–340	209	1	32.13 (33.04)		−Loss of NO$_3$ and C$_8$H$_{10}$F$_2$O$_4$	UO$_2$	218(−), 526(−)
	340–650	525	1	25.10 (24.56)	57.02 (57.60)	−Loss of C$_{11}$H$_{14}$N$_3$O		

n^* = number of decomposition steps.

exhibits a band at 21,512 cm^{-1}, which may be assigned to the $^6A_{1g} \rightarrow T_{2g}(G)$ transition in octahedral geometry of the complex [23,32]. The $^6A_{1g} \rightarrow {}^5T_{1g}$ transition appears to be split into two bands at 12,845 and 15,758 cm^{-1}. The spectrum shows also a band at 28,089 cm^{-1} which may be attributed to ligand to metal charge transfer. The diffused reflectance spectrum of the Co(II) complex gives three bands at 15,480, 12,723 and 14,492 cm^{-1}. The bands observed are assigned to the transitions $^4T_{1g}(F) \rightarrow {}^4T_{2g}(F)$ (ν_1), $^4T_{1g}(F) \rightarrow {}^4A_{2g}(F)$ (ν_2) and $^4T_{1g}(F) \rightarrow {}^4T_{1g}(P)$ (ν_3), respectively, suggesting an octahedral geometry around Co(II) ion [23,32,33]. The region at 28,585 cm^{-1} refers to the charge transfer band. The diffused reflectance spectrum of the Ni(II) complex displays three bands at ν_1: 13,390 cm^{-1}: $^3A_{2g}(F) \rightarrow {}^3T_{2g}(F)$, ν_2: 14,792 cm^{-1}: $^3A_{2g}(F) \rightarrow {}^3T_{1g}(F)$ and ν_3: 20,492 cm^{-1}: $^3A_{2g}(F) \rightarrow {}^3T_{1g}(P)$ [23,32]. The spectrum shows also a band at 27,024 cm^{-1} which may be attributed to ligand to metal charge transfer.

The reflectance spectrum of the Cu(II) chelate consists of bands at 14,590 and 20,790 cm^{-1} which can be attributed to the ^2E_g and $^2T_{2g}$ transition normally observed for octahedral Cu(II) complex [23,32]. An intense peak observed at 25,055 cm^{-1} is due to ligand to metal charge transfer transition [32].

3.7. Thermal analyses

Thermogravimetric studies (TG) for the complexes were carried out within a temperature range from room temperature up to 800 °C. TG results are in a good agreement with the suggested formulae resulted from microanalyses data (Table 1). The determined temperature ranges and percent losses in mass of the solid complexes on heating are given in Table 4, which revealed the following findings:

The TG curve of LFX drug exhibits a first estimated mass loss of 45.02% (calcd. 44.98%) at 200–345 °C, which may be attributed to the liberation of C$_{10}$H$_{10}$N$_2$ molecule as gases (Table 3). In the second estimated mass loss of 54.59% (calc. 54.94%), at 345–620 °C, which may be attributed to the liberation of C$_7$H$_9$F$_2$NO$_3$ molecule as gases.

The [Fe(LFX)(Gly)(H$_2$O)$_2$]Cl$_2$·H$_2$O complex gives a decomposition pattern as follows; the first stage is one step within the temperature range of 50–220 °C, representing the loss of H$_2$O (hydrated) with a found mass loss of 5.40% (calcd. 5.77%). The second step represents the loss of two coordinated water and Cl$_2$ gases with a mass loss of 17.47% (calcd. 17.14%). The subsequent step represents the loss of the remaining part of the complex with mass loss of 64.41% (calcd. 64.28%). At the end of the thermogram, the metal oxide Fe$_2$O$_3$ was the residue 12.27% (calcd. 13.02%), which is in good agreement with the calculated metal content obtained and the results of elemental analyses (Table 4).

The [Ni(LFX)(Gly)(H$_2$O)$_2$]Cl·H$_2$O complex is thermally decomposed in four stages. The first stage corresponds to a mass loss of 4.59% (calcd. 3.13%) within the temperature range 30–150 °C represents the loss of one molecule of hydrated water. The second stage corresponds to a mass loss of 24.90% (calcd. 25.50%) within the temperature range 150–250 °C and represents the loss of two coordinated water molecules, HCl and decomposition of organic part of the complex. The third and fourth stages, 250–655 °C, with a found mass loss of 49.48% (calcd. 50.48%) is reasonably accounted for decomposition of the remaining organic part of the complex leaving out NiO as a residue with a found mass loss of 21.01% (calcd. 20.89%).

The [Cu(LFX)(Gly)(H$_2$O)$_2$]Cl·2H$_2$O complex is thermally decomposed in four stages. The first stage corresponds to a mass loss of 3.69% (calcd. 3.11%) within the temperature range 40–115 °C and represents the loss of a molecule of hydrated water. The second stage corresponds to a mass loss of 22.90% (calcd. 22.87%) within the temperature range 115–255 °C and represents the loss of two coordinated water molecules, HCl and decomposition of organic part of the complex. The last two stage, 255–695 °C with a found mass loss of 60.35% (calcd. 60.85%), is reasonably accounted for the decomposition of the remaining organic part of the complex leaving out CuO as a residue with a found mass loss of 13.58% (calcd. 13.64%).

[UO$_2$·(LFX)(Gly)](NO$_3$) chelate exhibits two steps of decomposition within the temperature range 50–650 °C. In the first step of decomposition within the temperature range 50–340 °C in which

Table 5
Thermodynamic data of the thermal decomposition of the ternary complexes.

Complex	Decomp. temp. (°C)	E^* (kJ mol^{-1})	A (s^{-1})	ΔS^* J K^{-1} mol^{-1}	ΔH^* (kJ mol^{-1})	ΔG^* (kJ mol^{-1})
[Fe(LFX)(Gly)(H$_2$O)$_2$]Cl$_2$·H$_2$O	50–220	63.88	56.51×10^6	−196.4	−92.74	55.78
	220–275	163.5	14.23×10^7	−116.9	−53.47	141.3
	275–580	197.6	13.65×10^8	−83.56	−124.3	132.1
[Ni(LFX)(Gly)(H$_2$O)$_2$]Cl·H$_2$O	30–150	55.04	1.63×10^9	−59.08	71.19	76.82
	150–250	64.08	2.34×10^7	−100.7	77.98	98.42
	250–655	96.27	7.76×10^6	−116.7	206.2	260.2
[Cu(LFX)(Gly)(H$_2$O)$_2$]Cl·2H$_2$O	40–115	24.22	4.14×10^9	−151.2	238.50	243.3
	115–255	35.14	1.90×10^5	−140.4	57.01	84.50
	255–695	103.2	4.22×10^{12}	−6.84	247.0	250.1
[UO$_2$(LFX)(Gly)]·(NO$_3$)	50–340	43.09	6.24×10^7	−94.42	179.2	203.3
	340–650	52.39	4.47×10^6	−120.9	101.3	154.7

NO$_3$ and C$_8$H$_{10}$F$_2$O$_4$ gases with an estimated mass loss of 32.13% (calcd. 33.04%) occurs. The second step within the temperature range 340–650 °C, involves liberation of C$_{11}$H$_{14}$N$_3$O molecule with an estimated mass loss of 25.10% (calcd. 24.56%).

3.8. Kinetic data

The kinetic and thermodynamic parameters of thermal degradation process have been calculated using Coats–Redfern and Horowitz–Metzger models [34,35]. Coats–Redfern relation [34] is as follows:

$$\ln[\ln(1-\alpha)/T^2] = \ln(AR/\beta E) - (E/RT) \qquad (1)$$

α represents the fraction of sample decomposed at time t, defined by: $\alpha = (w_o - w_t)/(w_o - w_\infty)$, where w_o, w_t and w_∞ are the weight of the sample before the degradation, at temperature t and after total conversion, respectively. T is the derivative peak temperature. β is the heating rate = dT/dt, E and A are the activation energy and the Arrhenius pre-exponential factor, respectively. A plot of $\ln[-(\ln(1-\alpha))/T^2]$ versus $1/T$ gives a straight line whose slope (E/R) and the pre-exponential factor (A) can be determined from the intercept.

The Horowitz–Metzger equation [35] is an illustrative of the approximation methods. These authors derived the relation:

$$\log[(1-(1-\alpha)^{1-n})/(1-n)] = E^*\Phi/2.303RT_s^2 \quad \text{for } n \neq 1 \qquad (2)$$

when $n = 1$, the LHS of Eq. (2) would be $\log[-\log(1-\alpha)]$. For a first order kinetic process the Horowitz–Metzger equation may be written in the form (Eq. (3)):

$$\log[\log(w_\alpha/w_\gamma)] = E^*\Phi/2.303RT_s^2 - \log 2.303 \qquad (3)$$

where $\theta = T - TS$, $w_\gamma = w_\alpha - w$, w_α = mass loss at the completion of the reaction; w = mass loss up to time t. The plot of $\log[\log(w_\alpha/w_\gamma)]$ versus θ was drawn and found to be linear from the slope of which E^* was calculated. The pre-exponential factor, A, was calculated from the Eq. (4):

$$E^*/RT_s^2 = A/[\phi \exp(-E^*/RT_s)] \qquad (4)$$

A number of pyrolysis processes can be represented as a first order reaction. The degradation of a series LFX complexes was suggested to be first order, therefore we assume $n = 1$ for the remainder of the present text. The other thermodynamic parameters such as activation energy (E), preexponential factor (A), entropy of activation (ΔS), enthalpy of activation (ΔH) and free energy of activation (ΔG) of decomposition steps were calculated using Coats–Redfern [34] and Horowitz–Metzger [35] methods and the average values obtained are listed in Table 5. From the results, the following remarks can be pointed out:

– The high values of the energy of activation of the complexes reveal the high stability of such chelates due to their covalent bond character [36].
– The positive sign of ΔG for the investigated complexes reveals that the free energy of the final residue is higher than that of the initial compound, and all the decomposition steps are non-spontaneous processes. Also, the values of the activation, ΔG increases significantly for the subsequent decomposition stages of a given complex. This is due to increasing the values of $T\Delta S$ significantly from one step to another which overrides the values of ΔH [36].

The negative values of ΔS for all the complexes indicate more ordered activated complex than the reactants or the reaction is slow [36].

The data listed in Table 5 show that the activation energy E^* change with the increase of atomic number in the 3rd series of d-block elements, for the first decomposition step of their complexes. The complexes of Fe(III) (d^5) and Ni(II) (d^8) present higher that of Cu(II) (d^9) complex. This means that these complexes are more stable at the beginning of the decomposition than those on the Cu(II) complex [37]. The same trend is gained for these complexes at the second steps of decomposition, except they become excited before decomposition. These quantitative explanations of results mean also that the thermal stability is mainly related to the stereo-structure of the complexes and the electronic configuration of the d-block elements. Therefore, pairing up energy P and energy of splitting of metal orbitals in octahedral Δ_0 in strong environment are calculated. It is obvious that, those elements of Fe(III) (d^5) (t$_{2g}^5$ eg^0, $\Delta_0 = -10/12 - P$) and Ni(II) (d^8) (t$_{2g}^6$ eg^2, $\Delta_0 = -6/12 - 2P$) are stable since they have high pairing up energy and even an electron system. The Cu(II) (d^9) (t$_{2g}^6$ eg^3, $\Delta_0 = 3/12$) has less stability due to the lower pairing effect. It can be concluded that, the relation between E^* vs. atomic number gives a quantitative interpretation to the thermal stability of the complexes [37].

3.9. X-ray powder diffraction

X-ray powder diffraction pattern in the $0° < 2\theta < 60°$ of the LFX and glycine ligands and their metal complexes were carried out in order to give an insight about the lattice dynamics of these complexes. The X-ray powder diffraction obtained reflects a shadow on the fact that each solid represents a definite compound of a definite structure which is not contaminated with starting materials. XRD analysis for ternary chelates shows that the coordination of LFX alone or in the presence of glycine to the metal ions changes the XRD pattern of the ligands. This means that the metal ions are not fitted in the same phase of LFX and glycine. Therefore, the non-similarity of XRD pattern between the metal ions and ternary chelates suggests that these chelates have a different phase
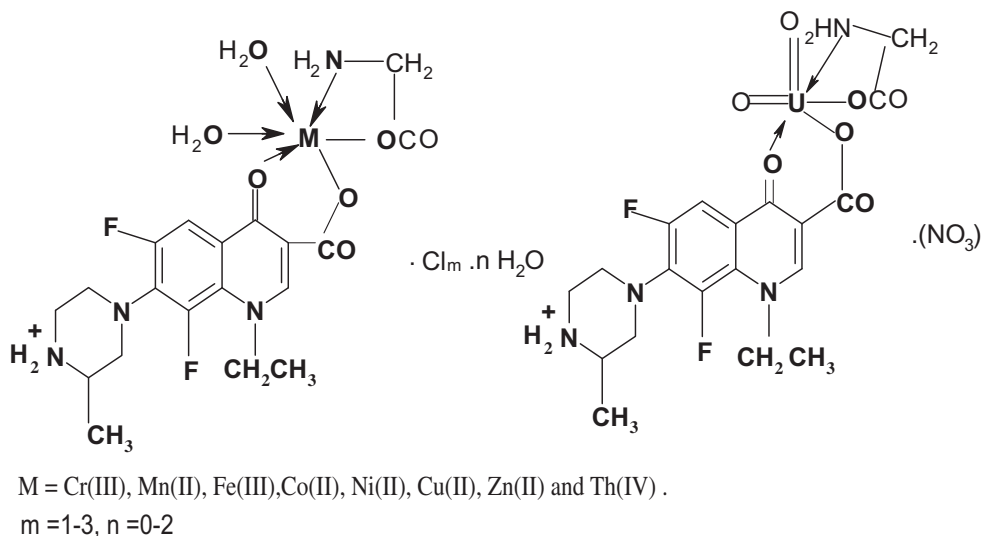
M = Cr(III), Mn(II), Fe(III),Co(II), Ni(II), Cu(II), Zn(II) and Th(IV) .
m =1-3, n =0-2

Fig. 4. Structures of metal complexes.

Table 6
Biological activity of ternary M—LFX—gly complexes.

Sample	Inhibition zone diameter (mm/mg sample)			
	E. coli	Neisseria gonorrhoeae	Staphylococcus aureus	Bacillus subtilis
Control: DMSO	0.0	0.0	0.0	0.0
Glycine	10	9	0.0	10
LFX	43		44	
[Cr(LFX)(Gly)(H$_2$O)$_2$]·Cl$_2$	40	45	43	44
[Mn(LFX)(Gly)(H$_2$O)$_2$]·Cl	42	45	40	41
[Fe(LFX)(Gly)(H$_2$O)$_2$]Cl$_2$·H$_2$O	44	47	46	46
[Co(LFX)(Gly)(H$_2$O)$_2$]·Cl	45	47	48	45
[Ni(LFX)(Gly)(H$_2$O)$_2$]Cl·H$_2$O	40	43	44	41
[Cu(LFX)(Gly)(H$_2$O)$_2$]Cl·2H$_2$O	40	42	40	42
[Zn(LFX)(Gly)(H$_2$O)$_2$]·Cl	46	44	42	47
[Th(LFX)(Gly)(H$_2$O)$_2$]·Cl$_3$	43	44	45	47
[UO$_2$(LFX)(Gly)](NO$_3$)·3H$_2$O	49	50	50	51
Standard Tetracycline	34	33	30	30
Order of activity	UO$_2$(II) > Zn(II) > Co(II) > Fe(III) > Th(IV) = LFX > Mn(II) > Ni(II) = Cu(II) = Cr(III) > tetracycline > glycine	UO$_2$(II) > Fe(III) = Co(II) > Mn(II) = Cr(III) > Zn(II) = Th(IV) > Ni(II) > Cu(II) > tetracycline > glycine	UO$_2$(II) > Co(II) > Fe(III) > Th(IV) > Ni(II) = LFX > Cr(III) > Zn(II) > Mn(II) = Cu(II) > tetracycline > glycine	UO$_2$(II) > Zn(II) = Th(IV) > Fe(III) > Co(II) > Cr(III) > Cu(II) > Mn(II) = Ni(II) > tetracycline > glycine

structures than the LFX and glycine ligands. In addition, on comparing the XRD spectra of the ternary chelates with the XRD spectra of the free ligands, indicate the crystallinity of the ternary chelates under study, except [Co(LFX)(Gly)(H$_2$O)$_2$]·Cl and [UO$_2$(LFX)(Gly)](NO$_3$) chelates, they can be considered as amorphous structure.

4. Structural interpretation

From all of the above observations, the structure of these complexes may be interpreted in accordance with ternary complexes of LFX drug and glycine with a similar distribution of like coordinating sites [19,24,27,28]. The structural information from the previously reported complexes is in agreement with the data reported in this paper based on the IR, molar conductivity, magnetic and electronic spectra measurements. Consequently, the structures proposed are based on octahedral geometry. The LFX drug always coordinates via the carbonyl O and the protonated O atoms forming a two binding chelating site and glycine behave as uninegative bidentate ligand with NO donor sites and coordinated to the metal ions via the amino group N and deprotonated carboxylic oxygen. The proposed general structures are shown in Fig. 4.

5. Biological activity

5.1. Antimicrobial activity

Metal complexes may affect living systems. This has been known for over a hundred years in respect of the curare-like activity in mammals of some metal ammines. The antibacterial activities of transition metal complexes have been extensively studied following the discovery that chelating agents inhibit growth of bacteria when complexed with many metals. To assess the biological potential of the synthesized compounds, the LFX and glycine ligands and their mixed metal complexes was tested against the selected bacteria strains. The antimicrobial data were collected in Table 6. The synthesized complexes were found to possess remarkable bactericidal properties, it is however interesting that the biological activity gets enhanced on undergoing complexation with the metal ions. Finally, to complete the evaluation of biological activity of the synthesized complexes, some comparison with the known standard antibiotic were performed and the data are collected in Table 6 and shown in Fig. 5 and Supplementary Fig. 6.

The biological activity against the two gram positive (Staphylococcus aureus and Bacillus subtilis) and gram negative bacteria (Escherichia coli and Neisseria gonorrhoeae) of the ternary metal
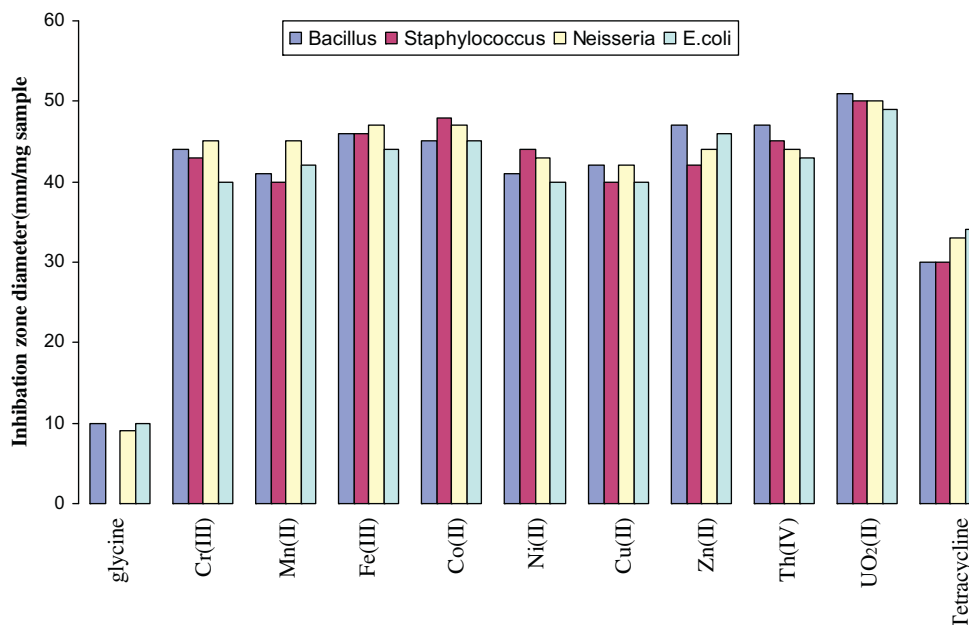
Fig. 5. Biological activity of LFX, Gly and ternary complexes.

Table 7
Cytotoxicity effect of ternary complexes.

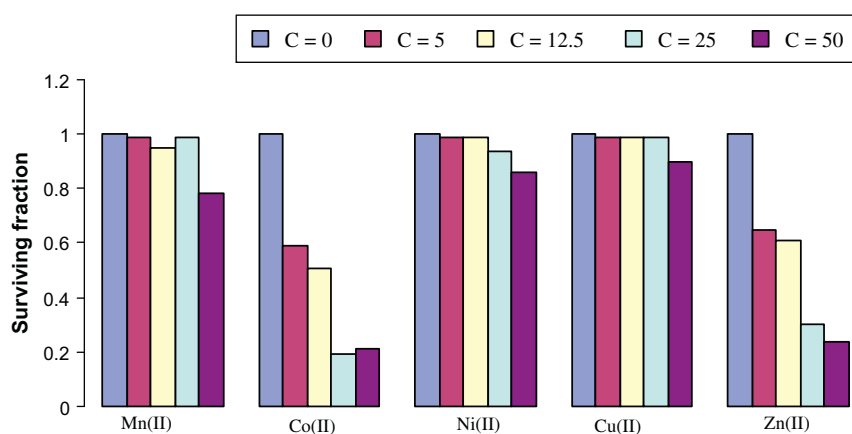| Complex	Surviving fraction (MCF7)					IC50 (µg/ml)
Concentration (µg/ml)	0.0	5	12.5	25	50	
LFX	1.00	0.64	0.53	0.27	0.19	14.0
[Mn(LFX)(Gly)(H$_2$O)$_2$]·Cl	1.00	0.99	0.95	0.99	0.78	11.2
[Co(LFX)(Gly)(H$_2$O)$_2$]·Cl	1.00	0.59	0.51	0.19	0.21	13.0
[Ni(LFX)(Gly)(H$_2$O)$_2$]Cl·H$_2$O	1.00	0.99	0.99	0.94	0.86	–
[Cu(LFX)(Gly)(H$_2$O)$_2$]Cl·2H$_2$O	1.00	0.99	0.99	0.99	0.90	–
[Zn(LFX)(Gly)(H$_2$O)$_2$]·Cl	1.00	0.65	0.61	0.30	0.24	16.8

Fig. 7. Anticancer activity of LFX and its ternary complexes.

complexes is higher than that of the LFX drug and glycine ligands and tetracycline standard. It is found that the activity increases upon coordination. The increased activity of the metal chelates can be explained on the basis of chelation theory [38]. The orbital of each metal ion is made so as to overlap with the ligand orbital. Increased activity enhances the lipophilicity of complexes due to delocalization of pi-electrons in the chelate ring [39]. In some cases increased lipophilicity leads to breakdown of the permeability barrier of the cell [38,39].

In Table 6, it is clear that although both of [Mn(LFX)(Gly)(H$_2$O)$_2$]·Cl and [Zn(LFX)(Gly)(H$_2$O)$_2$]·Cl complexes are nearly similar (except difference in ions where both of ions have II valance state), the inhibition zone diameter for *B. subtilis*, *S. aureus*, *N. gonorrhoeae* and *E. coli* are different. The antimicrobial mechanism of zinc complexes involves the capability of zinc ions to inhibit glycolysis of microorganisms by oxidizing thiols groups in essential glycolytic enzymes. It is therefore suggested that the potentiation of bacterial killing activity of Zn complex may be due to facilitation of entry of zinc ions into the inside of bacterial cells [40]. In addition, in biological systems, only manganese ion is readily capable of replacing Mg(II), but only in a limited set of circumstances. Mn(II) effectively binds ATP and allows hydrolysis of the energy molecule by most

ATPases. Mn(II) can also replace Mg(II) as the activating ion for a number of Mg(II)-dependent enzymes, although some enzyme activity is usually lost [40]. Sometimes such enzyme metal preferences vary among closely related species: for example, the reverse transcriptase enzyme of lentiviruses like HIV, SIV and FIV is typically dependent on Mg(II), whereas the analogous enzyme for other retroviruses prefers Mn(II) [41]. Also according to the chelation theory [38], the difference in activity between the two metal ions (Mn(II) had d^5 and Zn(II) had d^{10} configurations) can be attributed to the difference in probability of the d orbitals to overlap with the ligand orbitals. Also it could be due to the difference in electronegativity, size of the metal ion and the intermediate complex formation.

5.2. Cytotoxic activity

The LFX drug, glycine and all their ternary metal complexes were tested for their activity against breast cancer cell line (MCF7) by using 100 µg/ml drug concentration. From these results, it is clear that LFX, [Mn(LFX)(Gly)(H$_2$O)$_2$]·Cl, [Co(LFX)(Gly)(H$_2$O)$_2$]·Cl, [Ni(LFX)(Gly)(H$_2$O)$_2$]Cl·H$_2$O, [Cu(LFX)(Gly)(H$_2$O)$_2$]Cl·2H$_2$O and [Zn(LFX)(Gly)(H$_2$O)$_2$]·Cl were found to be very active against breast cancer cells with inhibition ratio values between 70% and 85.5%, while other complexes utilized in this work had been shown to be inactive (less than 70% inhibition). It is clear that a pattern of activity can be determined using different drug concentrations (Table 7). LFX, [Mn(LFX)(Gly)(H$_2$O)$_2$]·Cl, [Co(LFX)(Gly)(H$_2$O)$_2$]·Cl and [Zn(LFX)(Gly)(H$_2$O)$_2$]·Cl were found to be very active with IC50 values 14, 11.2, 13 and 16.8, respectively, while glycine and other complexes had been shown to be inactive at lower concentration than 100 µg/ml (Fig. 7).

6. Conclusion

The lomefloxacin drug (LFX) and its transition metal complexes with glycine have been prepared and fully characterized using the different spectral and physicochemical studies. The LFX drug has several coordinating sites which are suitably spatially arranged to bind transition metals which require hexa-coordination and glycine as essential amino acid behaves as a uni-negative bidentate ligand with NO donor sites and coordinated to the metal ions via the amino group N and deprotonated carboxylic oxygen. Significantly, further investigations on their antitumor activity revealed that such complexes possessed a considerable antitumor activity which was thought to be related with its DNA-binding affinity. The better binding properties of the complexes should be attributed to the good coplanarity of the ligand after coordination with metal ions. Meanwhile, nature of the central metal ions also affected the intercalative ability. Further study of complexes based on LFX as antibacterial drug is ongoing in our group.

Acknowledgments

Appendix A. Supplementary material

References

[1] A. Garoufis, J. Hatiris, N. Hadjiliadis, J. Inorg. Biochem. 41 (1991) 195–203.
[2] F.J. Pesch, H. Prent, B. Lippert, Inorg. Chim. Acta 169 (1990) 195–200.
[3] R.P. Rabindra, K. Sudhakar, Indian J. Chem. A29 (1990) 1182.
[4] R.P. Rabindra, R.M. Raviprakash, Indian J. Chem. A30 (1991) 1182.
[5] H. Sigel, B.E. Fisher, S. Farkas, Inorg. Chem. 22 (1983) 925–934.
[6] M. Sabat, K.A. Satyashur, M. Sundaralingam, J. Am. Chem. Soc. 105 (1983) 976.
[7] M.V.N. de Souza, M.V. de Almeida, Curr. Med. Chem. 10 (2003) 21–39.
[8] I. Turel, Coord. Chem. Rev. 232 (2002) 27–47.
[9] M. Ruiz, R. Ortiz, L. Perelló, S. García-Granda, M.R. Díaz, Inorg. Chim. Acta 217 (1994) 149–154.
[10] M. Ruiz, L. Perelló, J. Server-Carrió, R. Ortiz, S. García-Granda, M.R. Diaz, E. Cantón, J. Inorg. Biochem. 69 (1998) 231–239.
[11] B. Macias, M.V. Villa, M. Sastre, A. Castiñeiras, J. Borrás, J. Pharm. Sci. 91 (2002) 2416–2423.
[12] Z.H. Chohan, C.T. Supuran, A. Scozzafava, J. Enzyme Inhib. Med. Chem. 20 (2005) 303–307.
[13] Z.H. Chohan, H. Pervez, A. Rauf, C.T. Supuran, Metal Based Drugs 8 (2002) 263–267.
[14] M.P. López-Gresa, R. Ortiz, L. Perelló, J. Latorre, M. Liu-González, S. García-Granda, M. Pérez-Priede, E. Cantón, J. Inorg. Biochem. 92 (2002) 65–74.
[15] J.R. Anacona, C. Toledo, Trans. Met. Chem. 26 (2001) 228–231.
[16] I. Turel, L. Golic, P. Bukovec, M. Gubina, J. Inorg. Biochem. 71 (1998) 53–60.
[17] I. Turel, I. Leban, N. Bukovec, J. Inorg. Biochem. 66 (1997) 241–245.
[18] Z.F. Chen, R.G. Xiong, J. Zhang, X.T. Chen, Z.L. Xue, X.Z. You, Inorg. Chem. 40 (2001) 4075–4077.
[19] L.M.M. Vieira, M.V. de Almeida, H.A. de Abreu, H.A. Duarte, R.M. Grazul, A.P.S. Fontes, Inorg. Chim. Acta 362 (2009) 2060–2064.
[20] I. Sakiyan, E. Logoglu, S. Arslan, N. Sari, Biometals 17 (2004) 115–120.
[21] P. Skehan, R. Storeng, J. Natl. Cancer Inst. 42 (1990) 1107–1112.
[22] M.M. Abd-Elzaher, J. Chin. Chem. Soc. 48 (2001) 153–158.
[23] G.G. Mohamed, N.E.A. El-Gamel, Spectrochim. Acta A 60 (2004) 3141–r3154.
[24] L.M.M. Vieira, M.V. de Almeida, M.C.S. Lourenço, F.A.F.M. Bezerra, A.P.S. Fontes, Eur. J. Med. Chem. 44 (2009) 4107–4111.
[25] V.L. Dorofeev, Chem. Acta 38 (2004) 45–49.
[26] S. Kumar, A. Rai, S.B. Rai, D.K. Rai, A.N. Singh, V.B. Singh, J. Mol. Struct. 791 (2006) 23–29.
[27] M.S. Refat, G.G. Mohamed, R.F. de Farias, A.K. Powell, M.S. El-Garib, S.A. El-Korashy, M.A. Hussien, J. Therm. Anal. Calor. 102 (2010) 225–232.
[28] M.S. Refat, G.G. Mohamed, J. Chem. Eng. Data 55 (2010) 3239–3246.
[29] S. Kasselouri, N. Hadjiliadis, Inorg. Chim. Acta 168 (1990) 15.
[30] L.J. Bellamy, The Infrared Spectra of Complex Molecules, third ed., Chapman and Hall, London, 1975.
[31] K. Nakamoto, Infrared Spectra of Inorganic and Coordination Compounds, New York, Wiley Interscience, 1970.
[32] F.A. Cotton, G. Wilkinson, C.A. Murillo, M. Bochmann, Advanced Inorganic Chemistry, sixth ed., Wiley, New York, 1999.
[33] H.F. Abd El-halim, M.M. Omar, G.G. Mohamed, Spectrochim. Acta A 78 (2011) 36–44.
[34] A.W. Coats, J.P. Redfern, Nature 201 (1964) 68–79.
[35] H.W. Horowitz, G.M. Jetzger, Anal. Chem. 35 (1963) 1464–1468.
[36] O.A. El-Gammal, Spectrochim. Acta A 75 (2010) 533–542.
[37] G.G. Mohamed, F.A. Nour El-Dien, A. El-Gamel, J. Therm. Anal. Calorim. 67 (2002) 135–146.
[38] G.G. Mohamed, M.H. Soliman, Spectrochim. Acta A 76 (2010) 341–347.
[39] A.N.M.A. Alaghaz, R.A. Ammar, Eur. J. Med. Chem. 45 (2010) 1314–1322.
[40] Eun-Kyoung Choi, Hye-Hyang Lee, Mi-Sun Kang, Byung-Gook Kim, Hoi-Soon Lim, Seon-Mi Kim, In-Chol Kang, J. Microbiol. 48 (2010) 40–43.
[41] J.A. Cowan, Introduction to the Biological Chemistry of Magnesium, Magnesium in biology – Wikipedia, the Free Encyclopedia.htm, VCH, New York, 1995.